*Science World Journal Vol. 20(No 4) 2025* https://dx.doi.org/10.4314/swj.v20i4.41
*www.scienceworldjournal.org*
*ISSN: 1597-6343 (Online), ISSN: 2756-391X (Print)*
*Published by Faculty of Science, Kaduna State University*

Full Length Research Article

# PRODUCTION AND CHARACTERIZATION OF ACTIVATED CHARCOAL FROM *BORASSUS AETHIOPIUM* SEED AND ITS APPLICATION ON DYE EFFLUENT

*Walifa Ahmed, Doris E.A. Boryo, Auwal A. Mahmoud

Department of Chemistry, Faculty of Science, Abubakar Tafawa Balewa University, Bauchi, Bauchi State, Nigeria

*Corresponding Author Email Address: walifaahmed@gmail.com

**ABSTRACT**
Activated carbon was produced from *Borassus aethiopum* seeds through chemical activation using $H_3PO_4$ and alternative agents at 400-600°C for 20-60 minutes. Characterization showed carbonized samples (0.439 g/cm³ density, 73% carbon content) developed effective porosity (0.470 cm³/g pore volume) compared to raw seeds (0.531 g/cm³, 85.4% carbon). The material demonstrated excellent dye removal (84.4-99% efficiency) at 4-26 g dosage. Effluent analysis revealed significant improvements post-treatment: turbidity decreased from 33.26 to 1.02 NTU, conductivity from 1340 to 78.50 µS/cm, and pH normalized from 12.50 to 6.00. COD and BOD were reduced from 139.60 to 38.30 mg/L and 78.30 to 11.64 mg/L, respectively, meeting WHO standards. FTIR analysis identified key functional groups (O-H at 3441 $cm^{-1}$, C=O at 1799.72 $cm^{-1}$) contributing to adsorption, which followed pseudo-second-order kinetics ($R^2 > 0.99$), indicating chemisorption dominance. SEM confirmed the development of porosity in activated samples versus non-porous raw seeds. *Borassus aethiopum* is an effective precursor for wastewater treatment with comprehensive characterization supporting its adsorption mechanism.

**Keywords**: Activated Carbon, Borassus aethiopum, Wastewater, Dye Removal, Adsorption, SEM.

## INTRODUCTION

The textile industry is a major consumer of water, generating approximately **40–65 liters of effluent per kilogram of fabric produced** (Manu and Chaudhari, 2002). A significant environmental challenge associated with this wastewater is the presence of synthetic dyes, which are highly visible, resistant to degradation, and often toxic or mutagenic (Weisburger, 2002).

To address dye pollution, various **physicochemical and biological treatment methods** have been explored, including coagulation, oxidation, and microbial degradation (Slokar and Le Marechal, 1998; Robinson et al., 2001; Forgacs *et al.,* 2004). While these techniques vary in efficacy, stricter environmental regulations have shifted focus toward **greener and cleaner technologies** (Hai *et al.,* 2007). However, such methods often entail higher operational costs. Hybrid systems—combining multiple approaches—offer a promising solution by balancing efficiency and affordability.

Among hybrid strategies, **activated carbon** stands out due to its **exceptional adsorption capacity, tunable porosity, and versatile surface chemistry** (Marsh and Rodríguez-Reinoso, 2006). Traditionally, activated carbons are used as a standalone adsorbent for dye removal (Kannan and Sundaram, 2001); they also function as a **catalyst or support material** in advanced treatment processes. Its surface oxygen groups, for instance, enhance catalytic activity (Rodríguez-Reinoso, 1998; Figueiredo and Pereira, 2009). The ability to **engineer its physical and chemical properties** further amplifies its potential for optimizing textile wastewater treatment.

In this work, the production and characterization of activated carbon from *Borassus aethiopum* for textile dye removal are reported. The activation process was optimized for maximum adsorption capacity. Furthermore, the evaluation of the material's performance in treating real textile effluent and adsorption mechanisms through kinetic modeling was elucidated.

## MATERIALS AND METHODS

### Sample Collection and Preparation

Mature seeds of *Borassus aethiopum* (African fan palm) were collected from multiple locations within Alkaleri Local Government Area (10°15'N, 10°20'E), Bauchi State, Nigeria. The collected seeds were immediately placed in high-density polyethylene (HDPE) bags (0.5 mm thickness) to prevent moisture absorption and contamination during transport. The washed sample was exposed to sunlight and dried for 3 days. The sun-dried samples were crushed into fine particles with a mechanical crusher to determine the size before carbonization. Dye wastewater was collected from the local pits at Maiduguri Bye-pass, Bauchi state.

All chemicals and reagents used for this work were of analytical grades, and the major equipment used is: turbidity meter, UV-Visible Spectrophotometer (model 752N by Searchtech instruments), Muffle furnace, Scanning Electron Microscope (SEM) (Jeol Ltd with model JSM-17600F, USA) for characterization.

### Preparation of carbonized adsorbent

The Carbonized adsorbent was produced according method described elsewhere (Sumrit *et al.,* 2015). Briefly, 200 g of the sieved *Borassu eathipium* seed was carbonized by placing it in an electric furnace at 500 °C and heating it for 30 minutes. After this, it was allowed to cool and labeled in an air-tight polyethylene bag.

### Chemical activation of the carbonized adsorbent

Fifty grams (50 g) of carbonized carbon was impregnated with 150 m of 0.5 m hydrochloric acid, placed in a furnace set at 500 °C, and heated for 60 minutes. cold water was used to wash the activated carbon produced and further dried for 60 minutes at 110 °C in an oven till a constant weight of activated carbon was obtained (Sumrit *et al.,* 2015).

*Science World Journal Vol. 20(No 4) 2025* https://dx.doi.org/10.4314/swj.v20i4.41
*www.scienceworldjournal.org*
*ISSN: 1597-6343 (Online), ISSN: 2756-391X (Print)*
*Published by Faculty of Science, Kaduna State University*

The percentage yield was calculated as follows:

$$Percentage\ Yield = \frac{W1-W2}{W1} x\ 100$$

Where,

$W_1$ = Weight of raw material
$W_2$ = Weight of Carbonized raw material

**Characterization of activated carbonized adsorbent**
**Determination of the bulk density of carbonized adsorbent**
A small quantity of charcoal carbonized at 400, 500, and 600 °C was taken and ground to powder; sieved and separately put into the density bottle and weighed. The weight and the volume of the density bottle were initially determined (Andi and Paulus, 2018). The bulk density was calculated using the following expression:

$$Bulk\ density = \frac{mass\ of\ carbon\ sample}{volume}$$

**Determination of ash content of carbonized adsorbent**
Ash content of the carbonized was determined as reported in literature (Rafie *et al.,* 2013). Briefly, 3 g of the carbonized sample was weighed and heated in open crucibles at 750 °C for 1.5 hours. The crucible was then cooled and reweighed. This was calculated as:

$$Ash\ percentage = \frac{Ash\ weight}{Oven\ dry\ weight} x\ 100$$

**Determination of moisture content**
One gram (1g) of the sample was weighed and heated in a watch glass at 105 °C for 2 hours. The heated crucible was cooled and re-weighed (Rafie et al., 2013)
.

$$Moisture\ percentage = \frac{Loss\ in\ weight\ on\ drying\ (g)}{Initial\ weight\ (g)} x100$$

**Determination of the percentage of carbon**
The percentage of carbon in the raw material was determined by removing the Ash percentage and Moisture percentage from 100 % (Anon, 2011).

$$Percentage\ Carbon = 100 - Percentage\ ash - percentage\ moisture$$

**Determination of Physicochemical Parameters of the Untreated and Treated Dye Effluent.**
The physicochemical analysis of the dye effluent was carried out on the untreated and treated samples with the activated carbon (*Borassus aethiopium*). Some of the parameters, such as temperature, turbidity, total dissolved solids (TDS), conductivity, BOD, COD, and pH, were carried out immediately after sampling, while others were carried out at the laboratory (Coughlin, 2015).

**Determination of pH of the dye effluent**
After calibrating the pH meter, the measurement was carried out by rinsing the electrode with distilled water before it was dipped into a 50 ml beaker containing the test samples (treated and untreated) (Ramesh, 2017).

**Temperature of dye effluent**
Temperature was determined by dipping a mercury-in-glass thermometer calibrated in degrees centigrade (°C) into the three (3) samples, it was allowed to stand for some minutes before the readings were recorded (Das, 2011).

**Turbidity of dye effluent**
Turbidity was measured using a DR 2000 (HACH) spectrometer. Freshly sampled dye effluent was filled into a 25 ml sample cell, and another containing sampled water was analyzed. The knob of the spectrophotometer was turned to a programmed number of turbidity, which is 750, and wavelength 450mm. The distilled water was inserted first into the cell holder, and the lid (cover) was closed. The knob for zero was pressed to standardize the instrument. After that, the sample was inserted into the cell holder, and the red button was pressed, and the result was displayed on the display screen in formazine turbidity unit (FTU=NTU).

**Total dissolved solids (TDS) of dye effluent**
In determining TDS, 200ml of distilled water and 100 ml of dye effluent were poured into two separate beakers. The TDS/conductivity meter was switched on, and its sensor rod was dipped into the beaker containing distilled water, which gave a reading of 0.00 mg/litre TDS. After that, the sensor rod was dipped into the second beaker containing dye effluent, and the TDS/Conductivity meter then displayed the TDS value in mg/litre for both treated and untreated samples (Neumann and Fatula, 2016).

**Electrical conductivity of dye effluent**
The electrical conductivity of the treated and untreated dye effluent samples was determined by dipping the electrode inside a measured volume in the beakers containing the solutions. The conductivity of the untreated dye effluent was read (Neumann and Fatula, 2016). The procedure was repeated for the treated dye effluent.

**Biological oxygen demand (BOD) of dye effluent**
The biochemical oxygen demand was determined using standard methods (WHO, 2010). The treated dye effluent in the BOD bottle was thoroughly aerated, after which 10 ml of dye effluent was diluted with considerable distilled water. DO determination was carried out as described above. The bottle was sealed and incubated in the dark for 5 days at 20 °C (Deng *et al.,* 2010). DO was determined again for the second time. The BOD is the difference between the two determined DO levels as indicated below:
DO = Dissolved oxygen found in the sample on the initial day (initial day may be termed day Zero).

1. Untreated dye effluent.
   $BOD_5$, mg $1.^{-1} = \frac{D_o - D_T}{P}$

2. Treated dye effluent with activated carbon
   $BOD_5$, mg $1.^{-1} = \frac{(D_o - D_T) - fx(B_o - B_T)}{P}$

Where;
$D_0$ = dissolved oxygen of diluted sample initial, mg/L at 20 °C.

*Science World Journal Vol. 20(No 4) 2025* https://dx.doi.org/10.4314/swj.v20i4.41
*www.scienceworldjournal.org*
*ISSN: 1597-6343 (Online), ISSN: 2756-391X (Print)*
*Published by Faculty of Science, Kaduna State University*

$D_T$ = dissolve oxygen of diluted sample after 5 days' incubation
P = decimal volumetric fraction of sample used (volume of sample used/total volume of the diluted sample.
Bo = dissolve oxygen of dye effluent control initially, mg/L
$B_T$ = dissolve oxygen of dye effluent control after incubation, mg/L
F = ratio of % dye effluent in diluted sample to % dye effluent in dye effluent control.

**Chemical oxygen demand (COD) of dye effluent**
COD is another measure of organic material contamination in dye effluent specified in mg/L. COD is the amount of dissolved oxygen required to cause chemical oxidation of the organic material in water. COD parameter was measured using COD Vials (COD 251-1500 mg/L, Merck Germany) (Agarwal *et al.,* 2006).

**Adsorption Kinetic Investigation**
Activated carbon (1000 mg) from *Borassus aethiopum* was mixed with 50 mL of dye effluent (50–125 mg/L) at 30°C with shaking. After 30 min, samples were filtered (Whatman paper), and dye concentration was measured via UV spectrophotometry (590 nm). The process was repeated at 50 mg/L with sampling at 20–100 min intervals.

**Adsorption kinetic models**
The pseudo-first order and second order models need to be tested to determine which model is in good agreement with the experimental adsorption capacity (qe) value, thus suggesting which model the adsorption system follows.

**Pseudo-first-order kinetic model**
The Pseudo-first-order kinetic model was determined using the equation below:

$$\ln(q_e-q_t) = \ln q_e - k_1 t$$

Where $q_e$ is the amount of adsorbate adsorbed at equilibrium, (mg/g), $q_t$ is the amount of solute adsorbed per unit weight of adsorbent at time, (mg/g), $k_1$ is the rate constant of pseud-first order sorption (1/h). A plot of in $(q_e-q_t)$ versus t gives a straight line with slope of k1 and intercept of in $q_e$.

**Pseudo-second-order kinetic model**
The Pseudo-second-order equation was expressed as:

$$\frac{t}{qt} = \frac{1}{k2q2e} + \frac{1}{qe}t$$

a plot of $t/q_e$ versus t gives $1/q_e$ was determined.

**RESULTS AND DISCUSSION**
**Effect of Carbonization on the Physical Properties of Uncarbonized and Carbonized *Borassu aethiopium***
The physical properties of uncarbonized and carbonized *Borassu aethipium* are presented in Tables 1 and 2.

**Table 1:** Physical properties of the uncarbonized Borassus aethiopium

| Physical properties | Uncarbonized *Borassus aethiopium* |
|---|---|
| Bulk density (g/cm$^3$) | 0.531 |
| Moisture content (wt%) | 4.7 |
| Ash content (wt%) | 2.3 |
| Percentage of carbon (%) | 85.48 |
| Percentage of yield (%) | 73.00 |

**Table 2:** Physical properties of the carbonized Borassus aethiopium

| Physical properties | Temperature (°C) | Carbonized *Borassus aethiopium* |
|---|---|---|
| Bulk density (g/cm$^3$) | 500 | 0.439 |
| Moisture content (wt%) | 600 | 11.5 |
| Ash content (wt %) | 500 | 2 |
| Percentage of carbon (%) | 500 | 73.00 |
| Percentage of yield (%) | 600 | 72.87 |

Effect of Carbonization on Bulk Density
The bulk density measurements in Tables 1 and 2 showed predictable variations. The uncarbonized *Barrisu aethiopicum* sample had a bulk density of 0.531 g/cm³, while carbonization at higher temperatures reduced it to 0.439 g/cm³. This decrease aligns with previous studies by Putshaka and Adamu (2009), who observed a similar trend in carbonized leather waste, sawdust, and lignite. The reduction is likely due to the material's high carbon content. Other studies, such as those by Ekebafe *et al.* (2017) and Efeobokhan *et al.* (2019), also reported lower bulk densities in activated carbons from rubber seed shells and plantain peels, suggesting that high temperatures enhance micropore formation within the carbon structure. Differences in feedstock properties may explain variations across studies.

Effect of Carbonization on Moisture Content
The raw material initially had a moisture content of 4.7%, but after carbonization at 600°C (20–60 min), it increased to 11.5% in *Barassu aethiopium*-derived activated carbon (Maina and Anuka, 2014). At 650°C, moisture levels dropped to 0.09–4.20%. Anisuzzaman *et al.* (2015) found a similar range (2.20–2.91%) in activated carbon from *Typha orientalis* leaves, attributing the post-activation moisture gain to atmospheric adsorption.

Effect of Carbonization on Ash Content
The raw materials' ash content was 2.3%, decreasing to 2.0% after carbonization at 500°C (Tables 1 and 2). Extended carbonization further reduced ash content. In contrast, Putshaka and Adamu (2009) reported higher ash levels (4.34–4.44%) in leather waste-derived activated carbon. Maina and Anuka (2014) observed a decline from 2.01% to 0.75% in *Canarium schweinfurthii*-based carbon when processed at 650°C for 60 min. Generally, charcoal ash content ranges between 0.5% and 5%, depending on feedstock.

Effect of Carbonization on Fixed Carbon Content
Fixed carbon was calculated by subtracting ash and moisture percentages from 100%. The uncarbonized sample had 85.48% fixed carbon, which dropped to 73.00% after carbonization (Tables 1 and 2). Despite this decrease, the material remained suitable for activated carbon production. Maina and Anuka (2014) reported an increase from 80% to 99% in *Canarium schweinfurthii* seeds carbonized at 350–650°C for 60 minutes, as higher temperatures reduce ash, moisture, and volatile matter.

*Science World Journal Vol. 20(No 4) 2025* https://dx.doi.org/10.4314/swj.v20i4.41
*www.scienceworldjournal.org*
*ISSN: 1597-6343 (Online), ISSN: 2756-391X (Print)*
*Published by Faculty of Science, Kaduna State University*

Effect of Carbonization on Percentage Yield

The yield reduced slightly from 73.00% at 500°C to 72.87% at 600°C (Table 2). This is mainly due to volatile matter release and minor moisture loss (Eric *et al.,* 2014). Anisuzzaman *et al.* (2015) found yields between 39.22% and 73.10% for *Typha orientalis* carbon, with higher yields linked to increased $H_3PO_4$ concentration. Conversely, Ariany *et al.* (2018) noted yield reductions from 50% to 35% (800–900°C, 120 min) in sugarcane bagasse and rambutan twig-derived carbon, indicating that higher temperatures and longer processing times decrease yield. Similarly, Maina and Anuka (2014) observed a drop from 86% to 65% when activation temperature rose from 350°C to 650°C after 60 minutes, reinforcing that volatile matter loss at elevated temperatures reduces yield.

**Physicochemical parameters of a dye effluent**

**Table 3:** Physicochemical parameters of a dye effluent before and after treatment with the synthesized activated carbon

| Properties | Effluent before treatment | After treatment with activated carbon | Permissible limit for effluent discarded (WHO) |
|---|---|---|---|
| Colour | Black | Colourless | Black |
| Odour | Pungent | Odourless | Odourless |
| Electrical conductivity (µ/s/cm) | 1340 | 78.50 | 100.0 |
| Density (g/cm$^3$) | 1.023 | 0.977 | 1.00 |
| TDS (mgL$^{-1}$) | 802 | 47.00 | 2100 |
| TSS (mgL$^{-1}$) | 0.235 | 0.0041 | - |
| Turbidity (NTU) | 33.26 | 1.02 | 5 |
| COD | 139.60 | 38.30 | 50mg/L |
| BOD | 78.30 | 11.64 | 30mg/L |
| Temperature ℃ | 30.40 | 30.10 | Below 40 |
| pH | 12.50 | 6.00 | 6 - 9 |

TDS - Total Dissolved Solids
TSS - Total Suspended Solids
BOD - Biological Oxygen Demand
COD - Chemical Oxygen Demand

**Electrical Conductivity (EC):**

EC reflects ion concentration, with higher values indicating salinity. The untreated sample recorded 1340 µS/cm, exceeding WHO (2010) limits (100 µS/cm), while the treated effluent measured 78.50 µS/cm, within permissible levels. EC serves as a proxy for mineral content and pollution extent (Neumann and Fatula, 2016).

**Total Dissolved Solids (TDS):**

TDS measures inorganic salts and dissolved substances. High TDS levels (802 mg/L in untreated vs. 47 mg/L in treated) pose salinity risks in irrigation. The untreated sample surpassed WHO (2010) limits, necessitating treatment.

**Total Suspended Solids (TSS):**

TSS levels were 0.235 mg/L (untreated) and 0.004 mg/L (treated). Comparatively, Suriyaprabha and Fulekar (2018) reported extreme TSS values (9140–21,220 mg/L), far exceeding WHO thresholds.

**Turbidity:**

Elevated solids increased turbidity (33.26 NTU untreated vs. 1.02 NTU treated), impairing water clarity and photosynthesis. The treated sample met the WHO's 5 NTU limit.

**Chemical Oxygen Demand (COD):**

COD indicates organic pollutant levels. The untreated effluent (136.60 mg/L) exceeded the WHO's 50 mg/L limit, while the treated effluent (38.30 mg/L) complied. High COD suggests toxicity and reduced dissolved oxygen (DO), endangering aquatic life (Yasar, 2012).

**Biological Oxygen Demand (BOD):**

BOD measures microbial oxygen consumption during organic matter decomposition. Untreated effluent (78.30 mg/L) surpassed permissible levels (<100–300 mg/L), whereas treated effluent (11.64 mg/L) was compliant. Elevated BOD correlates with lower DO, stressing aquatic ecosystems (Rahman, 2011).

Morphological and Compositional Modifications

The micrograph of the untreated and activated carbon from *Borassus aethiopiumare* is presented in Figures 4 and 5, respectively.

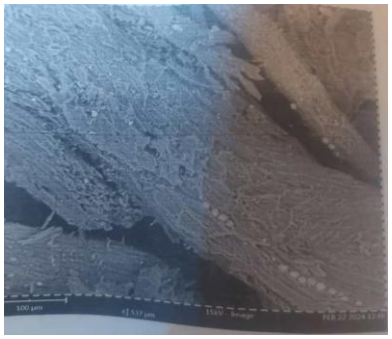

**Figure 1:** SEM Micrograph of uncarbonized Barassu aethopium seed (magnification = 1000)

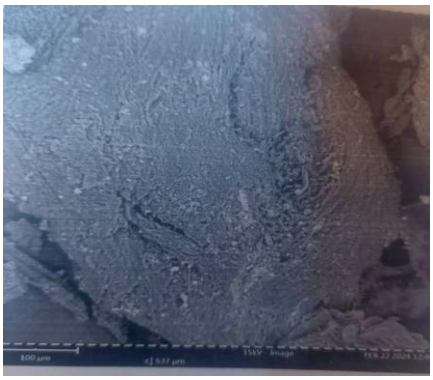

***Figure 2:*** *SEM Micrograph of carbonized Barassu aethopium seed (magnification = 1000)*

SEM micrographs revealed that raw *Borassus aethiopium* lacked porosity (Figure 1), whereas carbonized samples (Figure 2) exhibited a rough, porous morphology with crystalline structures.

*Science World Journal Vol. 20(No 4) 2025* https://dx.doi.org/10.4314/swj.v20i4.41
*www.scienceworldjournal.org*
*ISSN: 1597-6343 (Online), ISSN: 2756-391X (Print)*
*Published by Faculty of Science, Kaduna State University*

These structural changes are attributed to acid activation and high-temperature carbonization, which create micropores and mesopores, as reported by Prakash *et al.* (2012). EDX analysis confirmed the dominance of carbon **(88.04 wt%),** with minor traces of nitrogen and silicon, corroborating findings by Isil (2016) for ACs used in sulfide removal. The high carbon content and developed porosity explain the material's superior adsorption capacity (Yagmur *et al.,* 2008).

Functional Group Dynamics

FTIR spectra identified critical functional groups influencing adsorption. The presence of **O-H (3441 cm⁻¹)** and **C=O (1799 cm⁻¹)** in acid-treated AC (Table 4) indicates oxygenated surface groups, which facilitate dye binding via hydrogen bonding and electrostatic interactions (Baccar *et al.,* 2012). The absence of these groups in uncarbonized samples (Table 6) underscores the role of chemical activation in introducing active sites, consistent with Solum *et al.* (1995).

***Table 4****: FTIR Analysis of carbonized sample of carbonized Barassu Aethoipium seed*

| Activated Carbon | FTIR Band | Standard FTIR absorption band range ($cm^{-1}$) | Interpretation of functional group |
|---|---|---|---|
| Hydrogen chloride acid-activated carbon | 3441.00 | 35 00-3000 | OH stretching of the hydrogen group |
| | 2969.96 | 30 00-2840 | $Sp^3$ C-H |
| | 2929.20 | 30 00-2840 | $Sp^3$ C-H |
| | 2517.24 | 33 00-2500 | OH stretch acid |
| | 1799.38 | 18 00-1770 | C=O stretch |

Adsorption Kinetics

The adsorption process followed **pseudo-second-order kinetics ($R^2$ = 0.9694)**, indicative of chemisorption (Ho and McKay, 1999). The poor fit of the pseudo-first-order model ($R^2$ = 0.04887) further supports this mechanism, as noted by Kumar *et al.* (2020) for methylene blue adsorption. The high regression coefficient of the second-order model suggests that dye removal is governed by surface complexation rather than diffusion (Khaled *et al.,* 2008).

**Pseudo-first-order kinetic model**

Figure 3 shows the linearized plot of pseudo pseudo-first-order model with the regression coefficient $R^2$ from the data obtained being 0.04887. Kumar *et al*. (2013) observed a regression coefficient value of 0.4998 adsorption of methylene blue onto activated carbon, and Liu *et al.* (2019) also observed a regression coefficient of 0.3984 adsorption of lead ions onto graphene oxide. The curve fitting plot of ln qe-qt versus t does not show good results for the entire adsorption period. Kumar *et al.* (2013) also observed linear plot of the adsorption of methylene blue does not fit well in the first order. The result is in agreement with the work of Bello *et al.* (2008), adsorption of methylene blue onto activated carbon derived from periwinkle shells, and also observed by Bello *et al.* (2012) whose adsorption is not well fitted, making a pseudo-first order using imperata cylindrical leaf powder activated carbon.

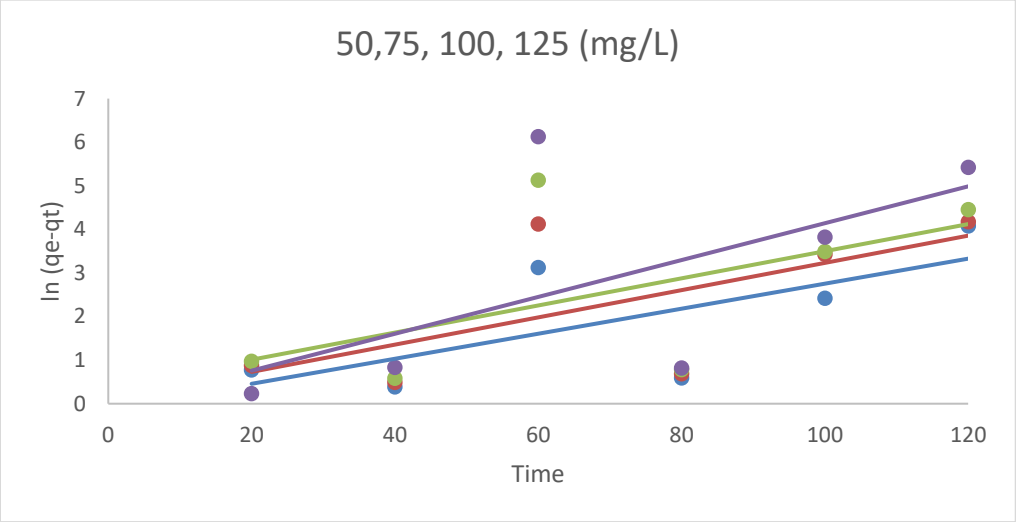


***Figure 3:*** *First-order plot of dye effluents adsorption*

**Pseudo-second order kinetic model**

Figure 4 showed the linearized plot of pseudo pseudo-second order model with the regression coefficient $R^2$ from the data obtained, 0.9694. The models with the highest regression coefficient $R^2$ have been considered the best model to explain the kinetic model from the data obtained. The value of the regression coefficient $R^2$ of the pseudo-second order model is higher than the pseudo-first order model, which shows that the pseudo-second order model is well fitted which indicating the absorption is limited by the chemisorption process. This is supported by Picking *et al.* (2011), who confirmed that pseudo-second order models as the most appropriate to fit the equilibrium experimental data due to a

higher value of coefficient of determination through error analysis compared to other adsorption isotherms, and also the plot gave a strong line for the dye concentration studied as shown. This confirmed the applicability of the pseudo-second order equation. This is in agreement with the work of Khaled *et al.* (2008), whose plot of t/qt versus t gave a straight line for all the initial dye concentration removal of direct N blue using activated carbon from orange peel.

Ahmad *et al.* (2014) discovered the regression coefficient $R^2$ value for the pseudo-second order kinetic model as 0.9842. The adsorption of RBBR dye onto PPAC followed the pseudo-second order kinetic model. This is due to greater competition for the adsorbent site at higher dye concentration (Ahmad *et al.* 2014).

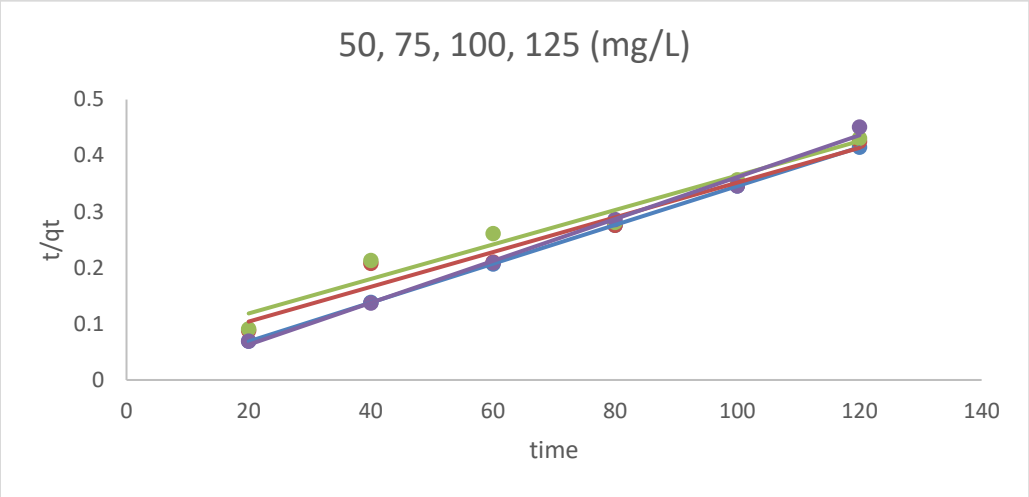


***Figure 4:*** *Second-order plot of dye effluents adsorption*

**Conclusion**

This research work was able to produce activated carbon that is cheap and eco-friendly using organic reagents on *Borassus aethiopium*. Various physical parameters like moisture content, bulk density, ash content, carbon content, and percentage yield of the charcoal were determined.

In addition, percentage decolouration of both the treated and untreated samples, various physical and chemical analyses of dye effluent, such as electrical conductivity, density, TDS, TSS, temperature, colour, and odor, were also determined.

The surface morphology of the activated carbon was reported using a scanning electron microscope (SEM), and the functional groups of the activated carbon were determined using Fourier transform infrared spectroscopy FTTR. The kinetic model shows that the experimental data can be well fitted by the pseudo-second order rate.

**REFERENCES**

Agarwal, R., Tandon, P., and Gupta, V.D. (2006). Phonon dispersion in poly (dimethylsilane). Journal of Organometallic Chemistry, 691(13): 2902-2908.

Ahmad M., Azreen N., Ahmed P., and Bello, O.S. (2014). Kinetic equilibrium and thermodynamic studies of synthetic dye removal using microwave-induced pomegranate KOH active. *Journal of Water Resource and Industry* 6, 18-35.

Andi, I.B., and Paulus, L.G. (2018). Characterization of active carbon prepared from coconut shell using FTIR, XRD, and SEM techniques. Albaruni Journal of Physics Education, 07(1): 33-39.

Anon, C. (2011). Ecological and toxicological association of dyes and pigments manufacturers, textile chemists, and colorists, German Ban of Use of Certain Azo Compounds in Some Consumer Goods. *ETAD Information Notice*, 6(28): 4-11.

Attia, A.A., Girgis, B.S. and Fathy, N.A. (2018). Dye pigment. *Journal of Chemical Engineering Science*, 76(1): 282-289.

Baccar, R., Blanquez, P., Bouzid, J., Feki, M., and Sarra, M. (2010). Equilibrium thermodynamic and kinetic studies on the adsorption of commercial dye by activated carbon derived from Olive-waste cake. *Journal of Chemical Engineering* 165(2); 457-464.

Bello, O.S. and Samire K. (2012). Equilibrium kinetic and quantum chemical studies on the adsorption of Congo Red using imperata cylindrical leaf powder activated. Toxicology and Environmental *Chemistry* (94) 1114-1124.

Bello, O.S., Adeogun, I.A., Ajadu, J.C., and Fehintola, F.K. (2008), adsorption of methylene blue onto activated carbon derived from periwinkle shells. Kinetic and equilibrium studies. *Chemical Ecology* 24; 285-295.

Coughline M. (2015). Treatment of textile effluent containing reactive red 120 dye using advanced oxidation**,** M.Sc. A Thesis, Dalhousie University, Halifax, Nova Scotia, 14.

Das, S. (2011). Textile effluent treatment: a solution to environmental pollution. http://www.fibre2fashion.com/industry-article/pdffiles/textile-effluent. Accessed on Feb. 2, 2011.

Deng H., Zhang G., Xu X., Tao G., and Dai J. (2010). Optimization of the preparation of activated from cotton stalk by microwave-assisted phosphoric chemical acid chemical activation. *Journal of Hazardous Materials*. **182**: 217-224.

Efeovbokhan, V.E., Alagbe, E.E., Odika, B., Babalola, R., Oladimeji, T.E., Abatan, O.G., and Yusuf, E.O. (2019).

Preparation and characterization of activated carbon from plantain peel and coconut shell using biological activators. *Journal of Physics*: Conference Series.

Ekebafe, L.O., Imanah, J.E., and Okieimen, F.E. (2017). Effect of carbonization on the processing characteristics of rubber seed shell. *Arabian Journal of Chemistry*, 10(1): 5174-5178.

Figueiredo, J.Ll. e Pereira, M.F.R. (2009). **Carbon as a catalyst**. In: serp, P., Figueiredo, J.L.(Eds.). Carbon Materials for Catalysis. John Wiley and Sons, Hoboken, NJ, pp. 177-217.

Forgacs, E., Cserhati, T. and Oros, G. (2004). Removal of synthetic dyes from wastewater: A review. *Environmental Journal*. 30: 953-971.

Hai, F.I., Yamamoto, K., Fukushi, K. (2007). Hybrid treatment systems for dye wastewater. *Critical Review on Environmental Science and Technology*. 37(4), 315-377.

Isil, I.G. (2016). Investigation of impregnated activated carbon properties used in hydrogen sulfide fine removal. *Brazilian Journal of Fuel Process Technology*, 64(1): 155-166.

Kaman, N. and Sundaram, M.M. (2001). Kinetics and mechanism of removal of methylene blue by adsorption on various carbons- a comparative study. *Journal of Dyes and Pigments*. 51(1), 25-40.

Khaled A, Ahmed E, Amany E, Ola A (2008). Removal of direct N Blue-106 from artificial textile dye effluent using activated carbon from orange peel. Adsorption isotherm and kinetic studies. *Journal of Hazardous Materials*, 2; 221-224.

Kumar, P.S., Ramalingam, S. (2013). Kinetic and thermodynamic studies of the adsorption of crystal violet dye on activated carbon. *Journal of Environmental Chemical Engineering,* **1**(3): 248-255.

Liu, Y., Y. Huang, A. Xiao, H. Qiu, and L. Liu (2019). "Preparation of magnetic Fe3O4/MIL-88A nanocomposite and its adsorption properties for bromophenol blue dye in aqueous solution," *Nanomaterials*, **9** (1). 123 - 142

Maina, N. S. and Anuka, A. A. (2014). Production of activated Carbon from atili seed shells. Retrieved on March 23, 2017, from https://lejpt.academicdirectorg/A25/gethtm.phphtm=195 209.

Manu, B. and Chaudhari, S. (2002). Anaerobic decolorisation of simulated textile wastewater containing azo dyes. *Bioresources Technology*. 82(3), 225-231.

Marsh, H. and Rodriguez-Reinoso, F. (2006). Activated Carbon, first ed. Elsevier, Oxford. Meng F., Chae, S-R., Drews, A., Kraume, M., Shin, H-S., Yang F., 2009. Recent advances in membrane bioreactors (MBRS): membrane fouling and membrane material. *Water Resources* 43(6), 1489-1512.

Neumann, S. and P. Fatula, (2016). Principles of Ion Exchange in Water Treatment. Techno focus. http://www.ionexchange.com/imperia/md/content/ion/presseschau/090316_asian_water_principles_of_ion_exchange_neuman_03_09_pdf. Accessed on Aug. 9, 2025.

Picking, D. (2011). Adsorption of Cu(II) ions onto a novel adsorbent material: kinetics, isotherms, and thermodynamics. *Journal of Hazardous Materials* **11**, 411-422.

Prakash, Nagapillai, S. Lathia, S., P.N., Sudha, Gopalan, and Renganathan (2012). Influence of day on the adsorption of heavy metals. *Environmental Science and Pollution Research*, **20**(2), 213 - 247

Putshaka, J.D. and Adamu, H.M. (2009). Production and characterization of activated carbon from leather waste, sawdust, and lignite. *Chemistry Search Journal* 1(1): 10-15.

Rafie, H.M. El-Rafie, and Zahran M.J. (2013). The Green synthesis of silver nanoparticles using polychararides extracted from Marine macroalgae. *Carbohydrate Polymer*. 25:96(2): 403-410.

Rahman, M.M., Bari, Q.H. and Yousuf, N.A. (2011). Treatment of textile wastewater with activated carbon produced from rice husk. Research Gate *online Journal*. Retrieved on June 5, 2019, from http://www.researchgate.net/publication/236115625

Ramesh B. B (2017). Photocatalytic degradation of a textile Azo dye, Sirius Gelb GC on $TiO_2$ Particles in the absence and presence of UV irradiation: the effects of some inorganic anions on the photocatalysis. Photochemistry and Photobiology A: *Chemistry*, 163 (1-2); pp. 29-35.

Robinson, T., McMullan, G., Merchant, R., and Nigam. P. (2001). Remediation of dyes in textile effluent: a critical review on current treatment technologies with a proposed alternative. *Bioresource Technology*. 77(3), 247-255.

Rodríguez-Reinoso, F. (1998). The role of Carbon materials in heterogeneous catalysis *Carbon* 36(3), 159-175.

Slokar, Y.M., and Le Marechal, A.M., (1998). Methods of decoloration of textile wastewaters. *Dyes Pigment* 37(4), 335-356.

Solum, M.S., Pugmire, R.J., Jagtoyen, M., and Derbyshire, F. (1995). Evolution of carbon structure in chemically activated wood. *Journal of Carbon*, 33: 1247-1254.

Sumrit M. (2015). Characterization and properties of activated carbon. A thesis submitted to the Department of Chemistry, Faculty of Science, Naresuan University, Phitsanulok, Thailand, Published 25th November.

Suriyaprabha, R. and Fulekar, M. H., (2018) Study on the physico-chemical parameters of dye industry effluents from industrial estate Vatva, Ahmedabad, Gujarat, *International Journal of Advanced Engineering and Research Development*, **5**(3): 1706-1710

Weisburger., J.H., (2002)., Comments on the history and importance of aromatic and heterocyclic amines in public health. *Mutation Re*search 506, 9-20.

World Health Organization (WHO) (2010). *Guidelines for Drinking Water Quality*. Vol. 2. Pp. 15-16.

Yagmur E., Ozmak M., and Aktas A. (2008). A novel method for the production of activated carbon from waste tea by chemical activation with microwave energy. *Journal of Fuel*. **87**(15): 3278-3285.

Yasar, A., Khalil, S., Tabinda, A.B., and Malik, A. (2012). Comparison of cost and treatment efficiency of solar-assisted advanced oxidation processes for textile dye bath effluent. *Korean Journal of Chemical Engineering*, 30(1), 131-138.